Journal of
Synchrotron
Radiation

ISSN 0909-0495

Received 30 November 2004
Accepted 14 April 2005

μGISAXS and protein nanotemplate crystallization: methods and instrumentation

Eugenia Pechkova,[a,b] Stephan V. Roth,[c] Manfred Burghammer,[d] David Fontani,[b] Christian Riekel[d] and Claudio Nicolini[a,b]*

[a]Fondazione ElBA, via delle Testuggini snc, I-00134 Rome, Italy, [b]Nanoworld Institute, Corso Europa 30, Genoa, Italy, [c]HASYLAB@DESY, Notkestraße 85, D-22603 Hamburg, Germany, and [d]ESRF, 6 rue Jules Horowitz, F-38043 Grenoble, France. E-mail: manuscript@nwi.unige.it

Microbeam grazing-incidence small-angle X-ray scattering (μGISAXS) has been used and the technique has been improved in order to investigate protein nucleation and crystal growth, assisted by a protein nanotemplate. The aim is to understand the protein nanotemplate method in detail, as this method has been proved capable of accelerating and increasing crystal size and quality as well as inducing crystallization of proteins that are not crystallizable by classical methods. The nanotemplate experimental setup was used for drops containing growing lysozyme crystals at three different stages of growth.

Keywords: protein nanocrystallography; microbeams; grazing incidence.

1. Introduction

Microbeam grazing-incidence small-angle X-ray scattering (μGISAXS) is a novel method of investigating locally thin films and surfaces (Müller-Buschbaum *et al.*, 2003; Roth *et al.*, 2003), giving access to length scales of up to several hundred nanometres. It is therefore a potentially very interesting technique for locally studying the growth of thin protein film and layers (Dante *et al.*, 1996) in the confined environment of a microdrop. The unique combination of a micrometre-sized beam with the reflection geometry allows us to gain, in principle, two orders of magnitude in spatial resolution compared with conventional GISAXS experiments, and thereby represents a very promising tool for probing protein crystal growth and nucleation at its very early stages, as induced by classical (Rosenberger, 1996) and nanotemplate-based (Pechkova & Nicolini, 2003; Pechkova & Nicolini, 2004) vapour diffusion methods. In the following article we will describe principally the methodological developments, aiming to demonstrate that scattering from a growing protein layer within a microdrop can be recorded.

2. Experimental methods

2.1. Microbeam grazing-incidence small-angle X-ray scattering

Experiments were performed at the microfocus beamline (ID13) of the ESRF (Riekel, 2000). The undulator beam was monochromated by an Si-111 double crystal to $\lambda = 0.9755$ Å, focused to a size of 25 μm × 12 μm (horizontal × vertical) by a double mirror and further collimated to 5 μm. A guard aperture in front of the sample was used to reduce parasitic scattering, and the beam intensity was calibrated by an ionization chamber. The geometry of the μGISAXS experiment is shown schematically in Fig. 1(*a*). The direct beam was blocked by a 300 μm-diameter cylindrical lead beamstop, and the specular beam located at $\alpha_f = \alpha_i$ (α_i is the incidence angle and α_f the exit angle) was blocked by a square lead beamstop of 4 mm edge length. The sample was mounted on an *xyz*-translation stage and a two-dimensional goniometer (α,ψ) allowed adjustment of the sample orientation [see Fig. 1(*a*) and Roth *et al.* (2003)]. Owing to the incident angle, $\alpha_i \simeq 1^\circ$, the beam footprint is enlarged in the *x* direction, leading to an actual beam size of ~300 μm × 5 μm (*x* × *y*). The scattering data were recorded using a two-dimensional charge-coupled detector (MAR CCD) with 2048 × 2048 pixels of size 64.45 μm × 64.45 μm and 16 bit readout. The sample-to-detector distance, L_{SD}, was calibrated to be 945.7 mm by an Ag–behenate standard (Blanton *et al.*, 1995).

A characteristic feature of a GISAXS pattern is the Yoneda (1963) peak (Y). This peak occurs at angles α_i, $\alpha_f = \alpha_c$, where α_c is the critical angle of the sample. The critical angle depends on the material *via* the real part of the refractive index and hence on the density and roughness of the layer. The relative intensities of the two Yoneda peaks can hence be interpreted in terms of a build up of layers, islands or holes.

Further analysis of the μGISAXS patterns is possible by two perpendicular cuts, which give access to the most prominent length scales. In so-called detector scans, the length scale vertical to the surface is probed. Here, basically at a fixed incidence angle α_i the exit angle α_f is varied at $\psi = 0^\circ$. The scattering from the surface can be related to correlated or uncorrelated roughness. A surface showing correlated roughness leads to well pronounced fringes along α_f in the

detector scan. This effect is called resonant diffuse scattering (Holy & Baumbach, 1994). In general, the thickness of the surfaces and thin films can be determined in this way.

2.2. Nanotemplate-based crystallization method

Protein samples to be studied were prepared on glass substrates of diameter 20 mm using the protein nanotemplate crystallization method (Pechkova & Nicolini, 2001, 2002*a*,*b*). In a typical experiment, a 10 µl drop containing lysozyme (20 mg ml^{-1}), 25 m*M* sodium acetate buffer (NaAc) with pH 4.5 and 0.45 *M* sodium chloride was placed on a siliconized glass slide covered with protein nanotemplate and stabilized over a reservoir of diameter 16 mm containing 0.9 *M* sodium chloride in sodium acetate buffer.

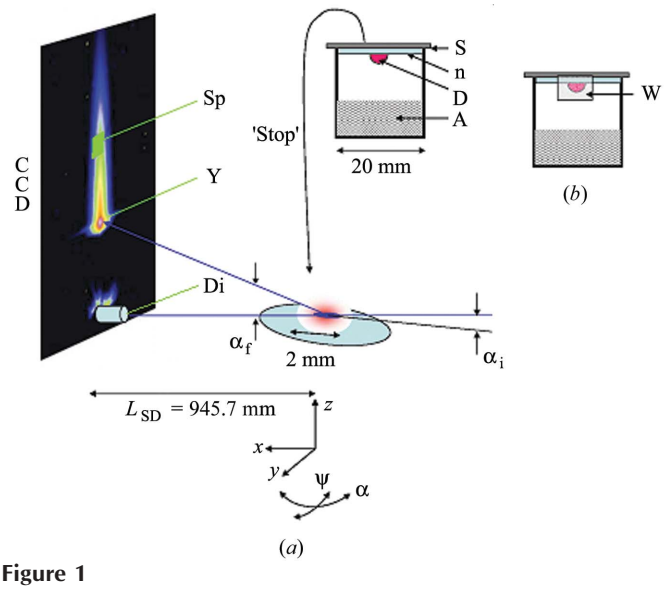

Figure 1
(*a*) µGISAXS and hanging-drop setup. The current hanging-drop setup is used for 'stop' experiments. Abbreviations: nanostructured protein template (n), substrate (S), protein solution droplet (D), precipitating agent (A). α_i and α_f denote the incident and exit angle; Sp is the specular reflected beam. The specular (Sp) and direct (Di) beams are shadowed by beamstops in order to avoid saturation of the detector. (*b*) Future setup for *in situ* experiments on nanocrystal growth with the hanging-drop technique. Thin X-ray transparent windows (W) allow entry and exit of X-rays.

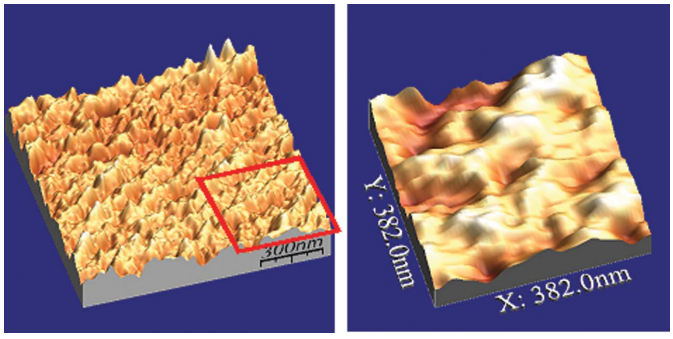

Figure 2
Images of the lysozyme template, obtained in tapping mode in a dry atmosphere (AFM: cantilever I type NSC14/Cr-Au MikroMash).

For these first methodological studies on protein nanotemplate crystallization, thin hen egg-white lysozyme film was used as nanotemplate, prepared on the water–air interface and compressed up to a surface pressure of 25 mN m^{-1} by means of a Langmuir–Blodgett trough. Two protein monolayers were deposited on the glass slide by the Langmuir–Schaeffer method. The protein template thus obtained was analysed by atomic force microscopy (AFM) (see below) in order to estimate the regularity and uniformity of deposition. The highly ordered protein nanotemplate was then utilized in the modified hanging-drop protein crystallization method, as shown schematically in Fig. 1(*a*). The drop was placed on the glass slide covered by the thin-film nanotemplate. As in the classical hanging-drop method, the glass slide with the protein template was sealed using vacuum grease (Pechkova & Nicolini, 2001, 2002*a*,*b*). The same crystallization conditions as for the classical hanging-drop method were applied. A series of 24 experiments were started at the same time in order that they might be stopped one after another, opening the crystallization chamber for the µGISAXS measurements. In this way, the sequence of different stages of crystallization allowed us to reconstruct the crystallization process in time. A comparison of the results obtained by the classical and nanotemplate methods will be presented elsewhere (Pechkova & Nicolini, 2005).

2.3. Atomic force microscopy

AFM is a topography-sensitive method, which can be used in certain cases in wet environments (Pechkova & Nicolini, 2002*b*). In its 'contact' mode, the tip at the end of the cantilever touches the sample. In the non-contact 'tapping' mode, AFM derives topographic information from measurements of attractive forces. Images of the lysozyme template have been obtained in tapping mode with a cantilever I type NSC14/Cr-Au MikroMash in a dry atmosphere utilizing an instrument based on the SPMagic controller built by Elbatech Srl (Pechkova & Nicolini, 2002*b*). The freeware *WSxM* (http://www.nanotec.es) was utilized for the processing of the acquired images. The typical resonance frequency of the cantilever tip is between 110 and 220 kHz, and the proper positioning of the cantilever on the AFM tip holder has been found at a frequency of 92 kHz, with intensity 0.6 V. The set point for loop control was at 0.2 V. The integral gain value during image grabbing has been set at 4.4 (*I* gain) and the proportional gain value during image acquisition has been set at 8.03 (*P* gain). Fig. 2 shows an AFM image of the superposed two layers of lysozyme acting as a nanostructured template for subsequent crystal growth.

2.4. Experimental protocol

The protein templates were freshly plated in the hanging-drop container during the three-day experiment. The glass substrate with the thin-film template and the droplet was removed from the container and the vacuum grease area was cleaned to ensure no contamination of the signal. The droplet existed for more than 60 min in air until complete evapora-

tion. Hence an optimum timing had to be found concerning the preparation, adjustment in the beam and data acquisition time. The glass substrate was subsequently brought into the beam and α_i was adjusted to about 1°. This procedure was restricted to less than 20 min in order to avoid precipitation of salt or nanocrystals from the solution to the substrate, which would lead to a contamination of the µGISAXS signal.

The droplet diameter was about 2 mm. Hence, the footprint of the X-ray beam was fully within the droplet diameter. The small beam size allows avoidance of excessive liquid scattering and provides, therefore, a reasonable signal-to-background ratio. The position of the drop relative to the beam was determined by an absorption scan with a photodiode. Experiments were performed with the beam at the centre of the droplet at the droplet–protein template contact area in order to optimize the signal of the weakly scattering biopolymer samples. Data collection times for individual droplets varied from 7 to 20 min. This interval is well below the minimum droplet evaporation time of about 60 min. This 'stop' procedure described above interrupts, therefore, crystal growth at specific times and allows the study of freshly grown thin films (see Fig. 1*a*)

3. Results and discussion

Fig. 3 shows an enlargement of the Yoneda region of the corresponding µGISAXS pattern. This region is most sensitive to structural and morphological changes of the surfaces owing to the interference effect involved in the occurrence of the Yoneda peak. The µGISAXS pattern is scaled to the same intensity. After 46 h, a new Yoneda peak (N) clearly emerges next to the Yoneda peak existing at shorter times (G), with a critical angle below that of the substrate. One could suppose that NaAc is precipitating on the substrate, thus leading to a new rough layer of small crystals. This outcome is unlikely for two reasons. The first is the rapid data collection after removal of the sample from the container. With the hanging-drop method itself, salt precipitation on the substrate should be reduced. In addition, this second peak does not appear at shorter times; one can calculate the nominal critical angle of NaAc using the known molecular mass and composition as $\alpha_c(\mathrm{NaAc}) = 0.23°$, which is larger than the critical angles of the glass and the protein. Hence, as a working hypothesis, one can attribute the peak at higher α_f values (G) to the glass substrate. The newly developing peak (N) thus seems to be related to the protein itself.

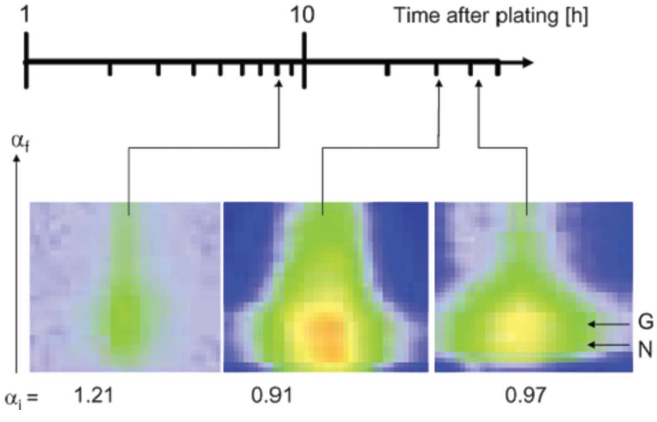

Figure 3
Development of Yoneda peak after plating (G) showing the development of a new peak (N) as a result of scattering from a protein layer (see text).

The occurrence of a second Yoneda peak indicates the development of a rough layer. Two models can be imagined, both competing to increase layer roughness (Fig. 4). In model A the roughness of the template layer is increased by holes: that is to say, this model assumes a decreasing density of the protein template layer as the layer itself is removed by the protein solution, thus triggering or assisting the formation of new crystals in the solution. Model B is motivated by a nucleation and growth process of possible protein nanocrystals on the nanostructured template, whereby protein molecules out of the solution might be adsorbed on the nanostructured template. At the present state of experiments we cannot favour model A or model B, *i.e.* a build up of holes or a layer of small islands, acting as nucleation centres for crystals. This question will be addressed in future *in situ* µGISAXS experiments based on scaled intensity data.

4. Outlook and conclusion

A feasibility study on template-assisted protein crystal growth using µGISAXS has been reported in this paper. The small droplet size used in hanging drop experiments necessitates the use of small X-ray beams and hence the µGISAXS technique. The recording of diffuse scattering implies measuring times of up to several minutes as a result of the intensity difference of several orders of magnitude between the specularly reflected and the diffuse scattering signal. Compared with bulk protein crystallography, the enlarged beam footprint results in less radiation damage. We have collected a time series of µGISAXS patterns and observed a stable µGISAXS pattern at least up to the first few images being acquired for the experiments reported here. It appears then that we can exclude that the surface morphology changes are due to beam damage, since the comparison among the different crystal-

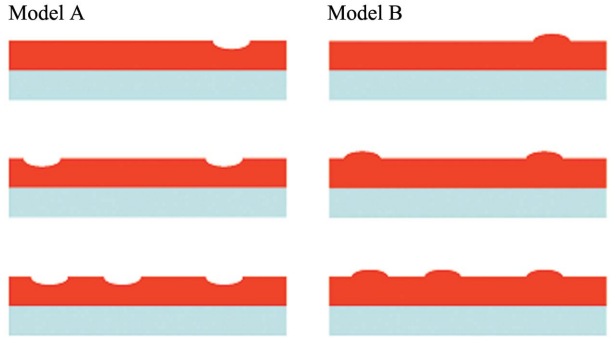

Figure 4
Two possible models for the increasing layer roughness with time. Model A favours increasing roughening *via* ablation of the nanostructured layer, while model B is nucleation-based.

lization time intervals after plating is made among corresponding patterns acquired consecutively. In future experiments one could also envisage translating the beam laterally across the substrate surface in order to limit radiation damage further.

Unlike topography-sensitive methods (*e.g.* AFM), μGISAXS exploits the penetration depth of X-rays. This allows investigation of the interface solution template, where significant signals were observed in the present case. Working with a droplet avoids time-consuming cleaning of the sample, *e.g.* salt removal. Thus the small remaining droplet is not hindering the measurement of the interface solution template, where nanocrystal growth is expected to take place. The technique of combining grazing-incidence with wide-angle scattering in order to really see crystallization (Bragg peaks) appears quite promising, and we plan to implement this technique in future *in situ* experiments.

Future experiments will be extended to *in situ* investigations of template-assisted protein growth, which provides several advantages. Thus crystal growth can be examined continuously. Furthermore, background subtraction will be facilitated and any contamination of the μGISAXS signal by cleaning or precipitating salt will be avoided. A possible setup, namely a hanging-drop container with thin entry and exit windows, is shown schematically in Fig. 1(*b*). This setup is the inverse of the traditional μGISAXS setup (Müller-Buschbaum *et al.*, 2003; Roth *et al.*, 2003) in order to obtain an upward-scattering geometry. This technique would, for the first time, allow one to follow protein crystal growth and nucleation from the very early stages after plating. Unlike for AFM, the hanging drop could be investigated by μGISAXS in its natural growth position without disturbing the growth process.

This work was supported by an FIRB–MIUR grant on Organic Nanoscience and Nanotechnology to the Nanoworld Institute, namely to the Centro Interuniversitario di Ricerca sulle Nanotecnologie e Nanoscienze Organiche e Biologiche of the University of Genoa, and to the Fondazione ElBA.

References

Blanton, T. N., Huang, T. C., Toraya, H., Hubbard, C. R., Robie, S. B., Louër, D., Göbel, H. E., Will, G., Gilles, R. & Raftery, T. (1995). *Powder Diffr.* **10**, 91–95.
Dante, S., Rosa, M. D., Francescagli, O., Nicolini, C., Rustichelli, F. & Troitsky, V. I. (1996). *Thin Solid Films*, **284–285**, 459–463.
Holy, V. & Baumbach, T. (1994). *Phys. Rev. B*, **49**, 10668–10676.
Müller-Buschbaum, P., Roth, S. V., Burghammer, M., Diethert, A., Panagiotou, P. & Riekel, C. (2003). *Europhys. Lett.* **61**, 639–645.
Pechkova, E. & Nicolini, C. (2001). *J. Cryst. Growth*, **231**, 599–602.
Pechkova, E. & Nicolini, C. (2002*a*). *J. Cell. Biochem.* **22**, 117–122.
Pechkova, E. & Nicolini, C. (2002*b*). *Nanotechnology*, **13**, 460–464.
Pechkova, E. & Nicolini, C. (2003). *Proteomics and Nanocrystallography*. New York: Kluwer.
Pechkova, E. & Nicolini, C. (2004). *Trends Biotechnol.* **22**, 599–602.
Pechkova, E. & Nicolini, C. (2005). *J. Cell Biochem.* In the press.
Riekel, C. (2000). *Rep. Prog. Phys.* **63**, 233–262.
Rosenberger, F. (1996). *J. Cryst. Growth*, **166**, 40–54.
Roth, S. V., Burghammer, M., Riekel, C., Muller-Bushbaum, P., Diethert, A., Panagiotou, P. & Walter, H. (2003). *Appl. Phys. Lett.* **82**, 1935–1937.
Yoneda, Y. (1963). *Phys. Rev.* **161**, 2010–2013.